J Neurophysiol 99: 734–746, 2008.
First published December 19, 2007; doi:10.1152/jn.01283.2007.

Olfactory Representations by *Drosophila* Mushroom Body Neurons

Glenn C. Turner,[1] Maxim Bazhenov,[2] and Gilles Laurent[1]
[1]*Division of Biology, California Institute of Technology, Pasadena; and* [2]*The Salk Institute for Biological Studies, La Jolla, California*

Submitted 27 November 2007; accepted in final form 17 December 2007

Turner GC, Bazhenov M, Laurent G. Olfactory representations by *Drosophila* mushroom body neurons. *J Neurophysiol* 99: 734–746, 2008. First published December 19, 2007; doi:10.1152/jn.01283.2007. Learning and memory has been studied extensively in *Drosophila* using behavioral, molecular, and genetic approaches. These studies have identified the mushroom body as essential for the formation and retrieval of olfactory memories. We investigated odor responses of the principal neurons of the mushroom body, the Kenyon cells (KCs), in *Drosophila* using whole cell recordings in vivo. KC responses to odors were highly selective and, thus sparse, compared with those of their direct inputs, the antennal lobe projection neurons (PNs). We examined the mechanisms that might underlie this transformation and identified at least three contributing factors: excitatory synaptic potentials (from PNs) decay rapidly, curtailing temporal integration, PN convergence onto individual KCs is low (~10 PNs per KC on average), and KC firing thresholds are high. Sparse activity is thought to be useful in structures involved in memory in part because sparseness tends to reduce representation overlaps. By comparing activity patterns evoked by the same odors across olfactory receptor neurons and across KCs, we show that representations of different odors do indeed become less correlated as they progress through the olfactory system.

INTRODUCTION

Understanding sensory learning requires some knowledge of the format of sensory representations in the networks where learning occurs and of the mechanisms by which these representations are stored or associated with other behaviorally relevant features (e.g., reinforcers, other sensory or motor representations). An example from the visual system illustrates the importance of representation format: the long-term memories of faces do not lie in the retina, although all the sensory information needed to construct face representations is originally present in the collective activity of ganglion cells. Individual ganglion cells can participate in the representation of all possible visual stimuli, from faces to moving bars. Changing synaptic strengths in the retina to store the memory of a specific face there would interfere with the representations of most other stimuli, making storage inefficient and imprecise. Rather the brain forms new often invariant representations of these objects in "higher" brain networks and in formats that are thought to be useful for storage and association (Logothetis and Sheinberg 1996; Quiroga et al. 2005; Tanaka 1996).

The olfactory system, with its relatively compact and shallow networks, offers a good opportunity to understand coding strategies optimized for learning. In vertebrates, only one layer, the olfactory bulb, separates the sensory neurons from olfactory cortex, an associative network. In insects, only the antennal lobe separates the sensory neurons from the mushroom body, a structure required for memory formation and retrieval (Erber et al. 1980; Heisenberg et al. 1985). As in the visual system, representations of olfactory stimuli in the sensory layer are distributed among a relatively small population of neurons. In *Drosophila*, there are only ~60 different types of sensory neurons (OSNs), many of which have well-characterized odor-response properties (Clyne et al. 1999; Gao and Chess 1999; Hallem and Carlson 2006; Robertson et al. 2003; Vosshall and Stocker 2007; Vosshall et al. 1999). Much like in the retina, a given sensory neuron carries information about many different stimuli; with the exception of special odors, such as pheromones [e.g., *cis*-vaccenyl acetate, carbon dioxide (Ha and Smith 2006; Schlief and Wilson 2007; Suh et al. 2004; van der Goes van Naters and Carlson 2007; Xu et al. 2005)], even monomolecular odors activate combinations of OSNs. Combinatorial representations are efficient encoding strategies particularly when the number of possible stimuli far exceeds the number of receptor types.

In *Drosophila*, olfactory sensory neurons project to the antennal lobe; OSNs of a given type converge in regions called glomeruli, where they contact projection neurons (PNs) and local interneurons. Inhibitory (Python and Stocker 2002; Wilson and Laurent 2005) and excitatory (Shang et al. 2007) local interneurons form widespread connections within the antennal lobe, whereas PNs convey olfactory information to deeper circuits in the brain, including the principal cells of the mushroom body, called Kenyon cells (KCs). The antennal lobe performs many important functions: because PNs of each type receive convergent inputs from ~40 OSNs of the same type, input noise can be reduced by signal averaging (Laurent 1999); using widespread local inhibition, the antennal lobe circuits can compress the dynamic range of its PN output over many orders of magnitude of input (Stopfer et al. 2003); and using local excitatory and inhibitory interactions, the antennal lobe broadens the tuning profiles of PNs relative to those of their cognate OSNs, making better use of coding space (Olsen et al. 2007; Wilson et al. 2004). These operations are important first steps in the processing of odor signals, ultimately favorable for odor discrimination. However, because PNs are broadly tuned, odor encoding at the level of antennal lobe output is densely combinatorial and thus inefficient for storage.

Classical lesion experiments (Erber et al. 1980; Heisenberg et al. 1985) and genetic blockade of KC synaptic output show that mushroom bodies are essential for memory formation and retrieval in fruit flies (Dubnau et al. 2001; Krashes et al. 2007; McGuire et al. 2001; Schwaerzel et al. 2002). In addition, many gene products with roles in learning are expressed at high levels in mushroom body neurons (Han et al. 1992, 1996,

Address for reprint requests and other correspondence: G. Laurent, Div. of Biology, California Institute of Technology, Pasadena, CA 91125 (E-mail: laurentg@caltech.edu).

The costs of publication of this article were defrayed in part by the payment of page charges. The article must therefore be hereby marked "*advertisement*" in accordance with 18 U.S.C. Section 1734 solely to indicate this fact.

1998; Nighorn et al. 1991). Nevertheless what forms olfactory memories and associations take remains essentially unknown. An essential step toward understanding this process is to determine how odors are represented across KCs. Previous studies of KC odor-response properties, using the genetically encoded Ca^{2+} sensor GCaMP, indicated that few KCs respond to a given odor (Wang et al. 2004). However, the sensitivity of the GCaMP sensor is low—typically a firing rate of 20 spike/s, sustained for ~1 s, is required for a detectable signal in vivo (Jayaraman and Laurent 2007; Pologruto et al. 2004; Wang et al. 2003). Under such conditions, many odor responses could go undetected; an electrophysiological approach sensitive enough to detect individual spikes and synaptic potentials or currents is clearly valuable.

This study details, for the first time, the representations of odors by mushroom body neurons in *Drosophila*, using in vivo whole cell recordings. We find that these cells have highly odor-selective responses and that odors are represented by sparse ensembles of neurons in the mushroom body. An important question is whether this sparseness could potentially facilitate learning by reducing the overlap between ensemble representations of different odors. We address this question directly by comparing representations across KCs with those across the sensory neurons, a comparison that is currently feasible only in *Drosophila*. We show that representations of different odors are on average less correlated in the mushroom body than in the primary sensory layer. Reducing correlations between different odor representations would diminish the problem of synaptic interference during learning and is likely to be a fundamental aspect of olfactory information processing at this level of the system.

METHODS

Preparation and olfactory stimulation

All flies were wild-type Canton-S females. For KC recordings, the animals were aged 1–2 days posteclosion; for PN recordings, they were 4–12 days old. They were raised on standard cornmeal medium (Lewis 1960). Flies were prepared for recording as described (Wilson et al. 2004) except that for KC recordings, the head was tilted forward to enable access to the posterior surface of the brain where the KC cell bodies are located. For KC recordings, flies were fixed in place using epoxy (Devcon 5 min epoxy). Cells were targeted for recording with IR-DIC optics under 400× magnification using an Olympus BX51WI with a 40× water-immersion objective.

Odors were delivered by injection of odorized air into a constant stream of carrier air. Two different stimulus conditions were used in the experiments in this study: 71 KCs were recorded under conditions that matched those used to characterize PN tuning curves (Wilson et al. 2004), and 40 KCs were tested with a different stimulation protocol where OSN responses have been most extensively characterized (Hallem and Carlson 2006). In the first stimulus protocol, a constant flow of air at 37.5 ml/s was directed at the fly's head. During odor stimulation, one 1/10 of this constant stream (3.75 ml/s) was diverted through a vial containing odorized air. Vials contained odor diluted 1:100 in paraffin oil (J. T. Baker), which, combined with the 1:10 dilution in the constant air stream, resulted in a 1:1,000 effective odor dilution. Six trials of each odor were delivered with a 500-ms stimulus duration and a 22-s interstimulus interval. Seventy-one KCs were recorded under these stimulus conditions, identical to those used to characterize PN tuning curves (Wilson et al. 2004).

To measure the separability of odor representations in KCs and OSNs (Fig. 5), we adjusted our stimulus protocol to match that in the study of Hallem and Carlson (2006) in which OSN responses have been most thoroughly characterized to date. Odors were diluted 1:100 in paraffin oil, as with the previous stimulation protocol; however, the flow of odorized air was increased to 5.9 ml/s, and the carrier air stream was decreased to 24 ml/s. Forty KC recordings were made with this odor concentration.

The 25 odors tested on KCs were: acetoin (CAS No. 513-86-0), benzaldehyde (100-52-7), 2-butanone (78-93-3), 2,3-butanedione (431-03-8), butyl butyrate (109-21-7), ethyl acetate (141-78-6), ethyl butyrate (105-54-4), ethyl propionate (105-37-3), geranyl acetate (105-87-3), 2-heptanone (110-43-0), 1-hexanol (111-27-3), *trans*-2-hexenal (6728-26-3), isoamyl acetate (123-92-2), linalool (78-70-6), 4-methylcyclohexanol (589-91-3), methyl salicylate (119-36-8), 3-methylthio-1-propanol (505-10-2), 3-octanol (589-98-0), 1-octen-3-ol (3391-86-4), pentyl acetate (53496-15-4), pentenal (1576-87-0), phenylethanol (98-85-1), propionic acid (79-09-4), 1-propanol (71-23-8), γ-valerolactone (108-29-2). The 33 odors tested on the PNs (Wilson et al. 2004) were benzaldehyde (100-52-7), 2,3-butanedione (431-03-8), 1-butanol (71-36-3), butyric acid (107-92-6), L-carvone (6485-40-1), cyclohexanol (108-93-0), cyclohexanone (108-94-1), 1,4-diaminobutane (110-60-1), ethyl butyrate (105-54-4), geranyl acetate (105-87-3), heptanal (111-71-7), 1-heptanol (111-70-6), 2-heptanone (110-43-0), hexanal (66-25-1), 1-hexanol (111-27-3), *trans*-2-hexenal (6728-26-3), *cis*-3-hexen-1-ol (928-96-1), isoamyl acetate (123-92-2), linalool (78-70-6), 4-methyl phenol (106-44-5), methyl salicylate (119-36-8), 3-methylthio-1-propanol (505-10-2), octanal (124-13-0), 1-octanol (111-87-5), 3-octanol (589-98-0), 2-octanone (111-13-7), 1-octen-3-ol (3391-86-4), pentyl acetate (53496-15-4), phenylacetaldehyde (122-78-1), propionic acid (79-09-4), 4-propyl phenol (645-56-7), pyrrolidine (123-75-1), γ-valerolactone (108-29-2). There were 16 odors tested on both PNs and KCs.

Whole cell recordings

In vivo whole cell patch-clamp recordings were performed as described previously (Wilson and Laurent 2005). For KC recordings, low-resistance recording pipettes with a high taper angle, but small (<0.5 μm) opening were shaped using the pressure polishing technique in which air (~35 psi) is forced down the lumen of the pipette while the tip is shaped with a heated platinum filament (Goodman and Lockery 2000; Lockery and Goodman 1998). Recordings were obtained using an Axoclamp-2B amplifier with a 0.01× headstage in bridge mode. Signals were filtered at 3 kHz and acquired at 10 kHz.

Extracellular saline contained (in mM) 103 NaCl, 3 KCl, 4 $MgCl_2$, 1.5 $CaCl_2$, 26 $NaHCO_3$, 5 N-tris(hydroxymethyl) methyl-2-aminoethane-sulfonic acid, 1 NaH_2PO_4, 10 trehalose, and 5 glucose. Saline osmolarity was adjusted to 275 mOsm with sucrose if necessary and equilibrated to pH 7.3 by constantly bubbling with a mixture of 95% O_2-5% CO_2. The preparation was continuously superfused with this solution throughout the recording (2 ml/min). The saline in the recording electrode contained (in mM) 125 L-K aspartate, 10 HEPES, 1.1 EGTA, 0.1 $CaCl_2$, 4 MgATP, 0.5 Na_3GTP, and 13 mM biocytin hydrazide (Invitrogen). We visualized biocytin labeling of KC processes using fluorescent conjugated streptavidin as described (Wilson et al. 2004).

Data analysis

All data analysis was performed with Matlab (The Mathworks, Natick, MA) or Igor Pro (WaveMetrics, Lake Oswego, OR). Spikes were identified based on their amplitude and sharpness using a time-derivative based algorithm custom written in Igor.

To assess whether a neuron responded to an odor, KC firing rates were measured in successive 200-ms bins and averaged across all trials. To qualify as a response, a KC's firing rate had to exceed 3.5 SD of baseline firing rate in a window 0–2 s after odor onset on at least half of the trials (typically 3 of 6 trials). We included this

reliability criterion because KC baseline firing rates are very low: one trial with several spikes could potentially qualify as a response. We used a slightly more conservative 4 SD threshold for PNs. To determine whether KC and PN tuning widths were significantly different, we used a bootstrap approach, creating mock distributions of tuning widths by sampling randomly with replacement from the tuning widths of 37 PNs. We compared these mock distributions with the observed distribution of KC tuning widths by *t*-test. In 10^5 iterations, all mock distributions were significantly different from the KCs.

Power spectral density (PSD) of the KC membrane potential waveforms was calculated with Thomson's multitaper method using Matlab routines from chronux.org. Odor-evoked power was determined by calculating the PSD of the signal during odor presentation. The valves controlling odor flow were opened for 500 ms. PSDs were analyzed for a 600-ms period beginning 100 ms after valve opening (because air flow rates introduce a delay in the arrival of the odor at the fly's) antennae, and subtracting from this the PSD during the same sized time window 10 s after stimulus presentation. Odor-evoked PSDs were calculated over the 10- to 55-Hz frequency range and averaged over all trials with a particular odor (5–15 trials) and normalized by the sum of the PSD in this bandwidth. Confidence intervals were at 0.01 (χ^2).

Sliding autocorrelations were calculated on KC membrane potential waveforms after band-pass (2–55 Hz) filtering and down-sampling from 10 to 1 kHz. Autocorrelation values for each trial were normalized to the maximum autocorrelation value for that trial, before averaging across all trials of an odor (5–15 trials).

We identified excitatory postsynaptic potentials (EPSPs) using a time-derivative-based algorithm. We measured EPSP frequencies in recordings of 27 different KCs. In a subset of 8 of those recordings, we blocked spiking activity by the addition of 1 μM TTX to the saline and calculated the frequency of mini EPSPs after the block. We constructed average waveforms from 49 well-isolated EPSPs (7 different KC recordings, and 7 EPSPs per recording) and 50 excitatory postsynaptic currents (EPSCs, 5 different recordings, 10 EPSCs per recording), identified by eye.

Population vectors were constructed to represent the responses of 24 different OSN types and 40 different KCs to a panel of eight odors. Responses of each OSN were the mean number of spikes during 1 s after odor onset, averaged over four to six different recordings for each OSN type. The responses of each KC were the mean spike rate across six odor trials from that KC, calculated in a 2-s epoch after odor. The angular separation between vectors representing two different odors was calculated as 1-cos(α), where α is the angle between the vectors.

Simulations

KCs were modeled as single-compartment neurons with channels governed by Hodgkin-Huxley kinetics: $C_m dV/dt = -g_L(V - E_L) - I^{syn}$, where C_m is the membrane capacitance, g_L is the leakage conductance, V is the membrane potential, E_L is the leak reversal potential, and I^{syn} is the sum of synaptic currents. Only passive membrane properties were simulated: $C_m = 1.0$ μF/cm^2, $g_L = 0.089$ mS/cm^2, $E_L = -57.8$ mV. Model parameters were tuned to produce the experimentally measured EPSP decay time constant: $\tau = 11.5$ ms.

Synaptic currents mediated by PN spikes were calculated according to $I^{syn} = g^{syn}[O](V - E^{syn})$, where g^{syn} is the maximal conductivity, $[O](t)$ is the fraction of open channels, and $E^{syn} = 0$ is the reversal potential. Synaptic currents were modeled by first-order activation schemes (Destexhe et al. 1994): $d[O]/dt = \alpha(1 - [O])[T] - \beta[O]$, where $[T]$ represents the concentration of transmitter (Bazhenov et al. 2001). $[T] = A\theta(t_0 + t_{max} - t)\theta(t - t_0)$, where $\theta(t)$ is the Heaviside (step-) function, $A = 0.5$, $t_{max} = 0.3$ ms (Destexhe et al. 1994). The rate constants, α and β, were estimated from voltage-clamp data using clampfit software (MDS Analytical Technologies): $\alpha = 2.5$ ms^{-1} and $\beta = 0.4$ ms^{-1}. Two values of the maximal conductance of PN-KC synapses were tested: $g_1 = 0.05$ mS/cm^2 to produce ESPS with amplitude 1.4 mV and $g_2 = 0.04$ mS/cm^2 to produce ESPS with amplitude 1.2 mV.

To test the effect of PN:KC convergence on KC spiking probability, a network of KCs ($n = 1{,}000$) was stimulated by PN input. PN spike times were taken from experimental data; different KCs in the network received input from different randomly selected sets of PNs. We assumed that a KC produces a spike when its membrane potential reaches the experimentally determined spike threshold $V_{th} = -36.3$ mV. KC spiking probability was then calculated for different values of PN:KC convergence ratio varying between 1 and 20.

RESULTS

Whole cell patch-clamp recordings of mushroom body KCs in vivo

We investigated olfactory responses in KCs using whole cell patch-clamp recordings in intact flies in vivo. KCs were targeted for recording using their characteristic location and small (2–3 μm), clustered cell bodies; identity was confirmed by dye filling. Input resistance at the soma was >10 GΩ; KCs were held at -58 ± 2 (SD) mV in current clamp. KCs showed abundant and mostly depolarizing PSPs in the absence of odor stimulation but very low spontaneous firing (0.1 ± 0.4 spike/s). Action potentials could be evoked by depolarizing current injection in every KC recorded and were typically <15 mV as recorded from the soma. They were effectively blocked by 1 μM tetrodotoxin (TTX), indicating that they are caused by sodium conductances (Fig. 1*A*).

We tested KC odor responses using a panel of 25 odors, presented at 1:1,000 dilution (1:100 in mineral oil and a further 1:10 dilution in a carrier air stream). We used this odor concentration to match that used previously with PNs and OSNs (Clyne et al. 1997; de Bruyne et al. 1999, 2001; Dobritsa et al. 2003; Wilson et al. 2004). This concentration is within the dynamic range of the OSNs (Hallem and Carlson 2006) and is similar to that used in the standard T-maze olfactory-foot shock learning protocol (Tully et al. 1994).

We obtained long-lasting recordings from 71 KCs at this odor concentration and tested each neuron with 10 odors on average, randomly selected from the panel of 25 (see METHODS). Whereas every KC had a synaptic response to at least one of the tested odors, spikes were evoked only rarely. Subthreshold responses could be depolarizing, hyperpolarizing or consist of overlapping or successive de- and hyper-polarizing epochs (Fig. 1, *B–D*). A given KC could exhibit very different subthreshold responses, depending on the odor presented. The KC in Fig. 1*B*, for example, was consistently depolarized in response to acetoin (3-hydroxy-2-butanone) and hyperpolarized in response to propionic acid. The KC in Fig. 1*C* was depolarized by both 2,3-butanedione and propionic acid but with consistently different profiles.

In some cases, a depolarizing response drove the membrane potential above firing threshold (Fig. 1*D,* pentenal). Examples of spiking responses, taken from selected KCs, are shown in Fig. 1, *E–H.* These responses were rare and comprised small numbers of spikes (sometimes as few as one per trial). We now examine KC response statistics and compare them to those of PNs, the source of their excitatory inputs from the antennal lobe.

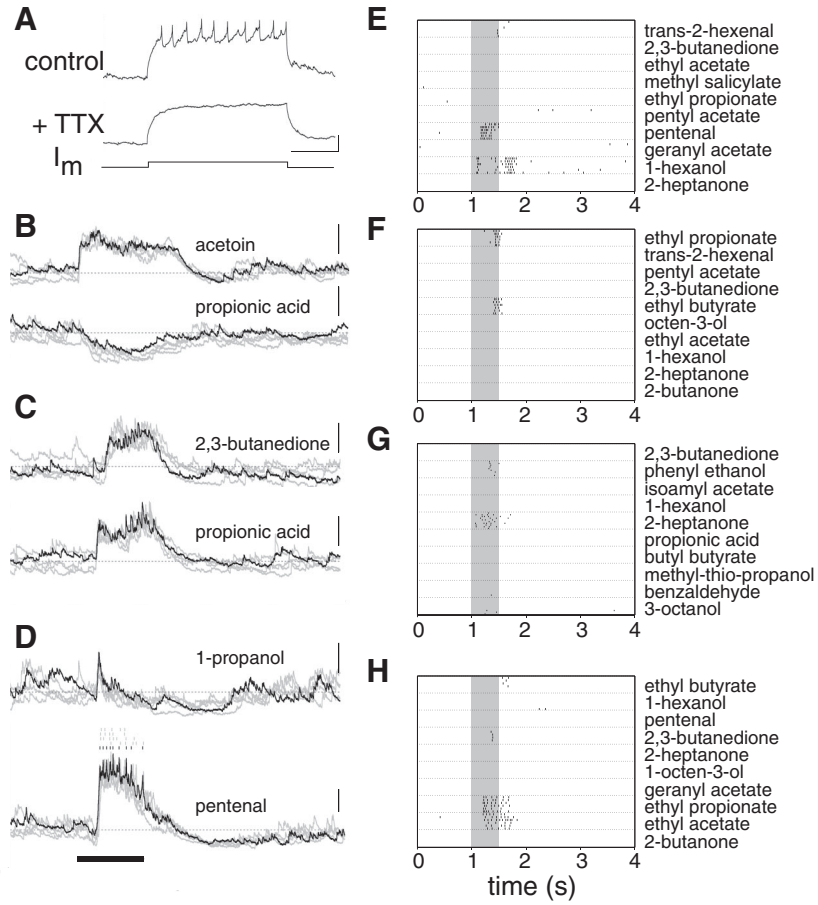

FIG. 1. Odor responses of Kenyon cells (KCs). *A*: whole cell patch-clamp recording of KC membrane potential. Current injection evokes TTX-sensitive action potentials. *B–D*: whole cell recordings of KC membrane potential during odor presentation, indicated by black bar. KCs exhibited a variety of subthreshold synaptic responses to odors. Suprathreshold spiking responses (*D, bottom*) were rare. Spike times during each trial, are indicated by tick marks above V_m. Voltage traces for multiple trials with the same stimulus are superimposed to illustrate consistency with one trace shown in black for clarity (scale bar = 10 mV). *E–H*: examples of spiking responses from 4 different KCs to a panel of different odors. Each odor is presented for 6 successive trials.

KC responses are sparse

We compared the density of odor responses in KCs to that in the antennal lobe PNs (Fig. 2, *A* and *B*). KCs were tested collectively with a panel of 25 different odors, PNs with 33. To estimate representation density, we measured the spiking response probability in KCs and PNs for each odor (equivalent to the fraction of neurons that respond to each odor). A KC was described as responsive if its firing rate crossed a threshold >3.5 SD above baseline at any time in the 2 s after odor onset (see METHODS). In our sample of 71 KCs, a given odor evoked a spiking response in only 6 ± 5% of the cells. PN response probability, by contrast, was 59 ± 14% (Fig. 2*A*, $n = 37$ PNs). These values are similar to those measured using tetrode recordings in the locust olfactory system where, using the same definition of a response, 11% of KCs and 64% of PNs responded to a given odor (Perez-Orive et al. 2002). Fourteen of the 71 analyzed *Drosophila* KCs did not fire a single spontaneous action potential during the entire recording session (note that all KCs could be driven to spike with current injection). Although these KCs all had clear subthreshold responses to odor, they would have gone undetected with extracellular recordings, possibly explaining the higher apparent response rate in locust experiments.

We next examined the tuning width of these two neuron populations. Each KC was tested with 10 odors on average (range: 6–14), and tuning width was measured as the fraction of those odors that evoked a spiking response. KCs were narrowly tuned, with 6 ± 12% of odors evoking a response in a given KC (Fig. 2*B*). PNs, by contrast, were broadly tuned: 53 ± 39% of odors evoke an excitatory response over all tested PNs. Note, however, that the distribution of PN tuning curve widths is bimodal (Fig. 2*B*): some PNs, possibly as many as 20%, are clearly specialists in *Drosophila*. PN and KC tuning-width distributions were statistically significantly different ($P < 10^{-5}$, see METHODS).

Different anatomical classes of KCs have different response properties

Drosophila KCs can be classified into three anatomical types based on their axonal projections (Crittenden et al. 1998; Lee et al. 1999). α/β and α'/β' KCs have bifurcating axons: one branch projects dorsally and forms the vertical lobe of the mushroom body (α, α'); the other extends medially to form the medial lobe (β, β'). α'/β' KCs are easily distinguished from α/β KCs by their projections to the thumb-like branch of the vertical lobe (α' lobe, arrow Fig. 2*C*). γ KCs have a single axon, contributing to the medial lobe. Previous work suggests that the three classes play different roles in memory formation, possibly because they connect to different postsynaptic targets (Akalal et al. 2006; Krashes et al. 2007; Pascual and Preat 2001; Zars et al. 2000). We examine here whether these morphological KC classes also differ physiologically.

α'/β' KCs were more broadly tuned than the other two types ($P < 0.05$, 1-way ANOVA). Overall, a trend of decreasing responsiveness could be detected from α'/β' to α/β to γ KCs, with statistically significant differences only

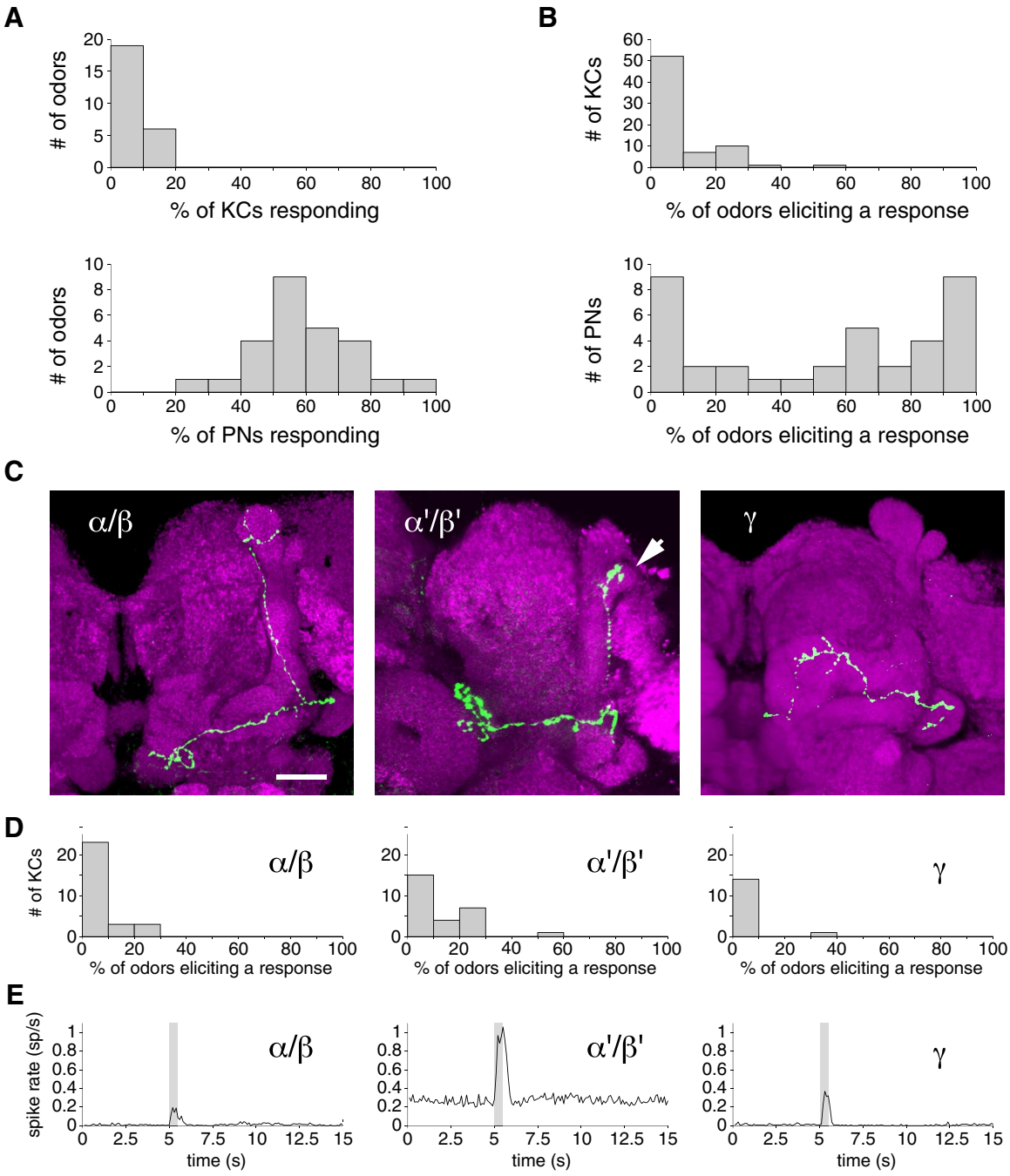

FIG. 2. Sparseness and response selectivity of KCs and projection neurons (PNs). *A*: distribution of responding-ensemble sizes in KCs (*top*) and PNs (*bottom*). The mean fraction of KCs that respond to a given odor is 6 ± 5% (n = 71), whereas in PNs it is 59 ± 14%, (n = 37). The firing-rate thresholds for counting excitatory responses were 3.5 SD (KCs) and 4 SD (PNs) above baseline. *B*: tuning widths for PNs and KCs measured as the fraction of tested odors that evoke a spiking response. KCs are more narrowly tuned than PNs (KCs: 6 ± 12%; PNs: 53 ± 39%). *C*: projection of confocal stacks showing representative axonal morphology of the 3 anatomical classes of KC. KCs (green) were filled with biocytin and visualized by fluorescent conjugated streptavidin. Brain neuropil (magenta) was stained using the nc82 antibody to identify and distinguish the different output lobes of the MB. α'lobe indicated by arrow. Scale bar = 20 μm. *D*: tuning widths of the different anatomical classes of KCs. KCs projecting to the α'/β' lobe showed a significantly higher response probability to the odors tested ($P < 0.05$, 1-way ANOVA). *E*: average response of different KC classes to all odors tested.

between γ and α'/β' KCs (Fig. 2*D*). Only 1 of the 15 γ KCs we tested with this odor set (and 1 of the 23 total γ KCs recorded at all odor concentrations) showed a spiking response to an odor, although all had detectable subthreshold responses.

We also computed the average instantaneous firing rate across all odors for all KCs of a given type (Fig. 2E). Average KC response profiles were single-peaked and closely followed the stimulus time course in all KC types. In addition to being more broadly tuned, α'/β' KCs had the highest baseline firing rate and the most vigorous responses to odors: they fired 4.9 ± 3.0 spikes during an odor response, significantly more than α/β KCs (2.2 ± 1.2; P = 0.007, t-test).

Synaptic drive from PNs to KCs

To examine how KCs integrate their inputs to achieve high odor selectivity, we analyzed synaptic events in these neurons. Our goals were to derive an understanding of synaptic integration by KCs and to estimate connectivity between the PNs and the KCs.

QUANTAL EVENTS. We characterized the amplitude, kinetics, and frequency of EPSPs in KCs held at 58 ± 2 mV (Fig. 3). EPSP rise time was short (~2 ms), allowing many synaptic events to be identified easily as peaks in the first time derivative of the membrane potential (Fig. 3*A*). These events were predominantly the result of spike-mediated synaptic vesicle release because their frequency dropped significantly when TTX was added to the saline (control: 19.8 ± 13.2 s^{-1}; TTX: 1.8 ± 1.3 s^{-1}, n = 8 KCs; Fig. 3*B*). TTX, however, did not change the mode of the EPSP amplitude distribution (Fig. 3*C*) and caused only a small change in its mean (control: 1.4 ± 0.8 mV; TTX: 1.0 ± 0.5 mV), resulting mainly from a decrease in the distribution's upper tail. We conclude that most spike-

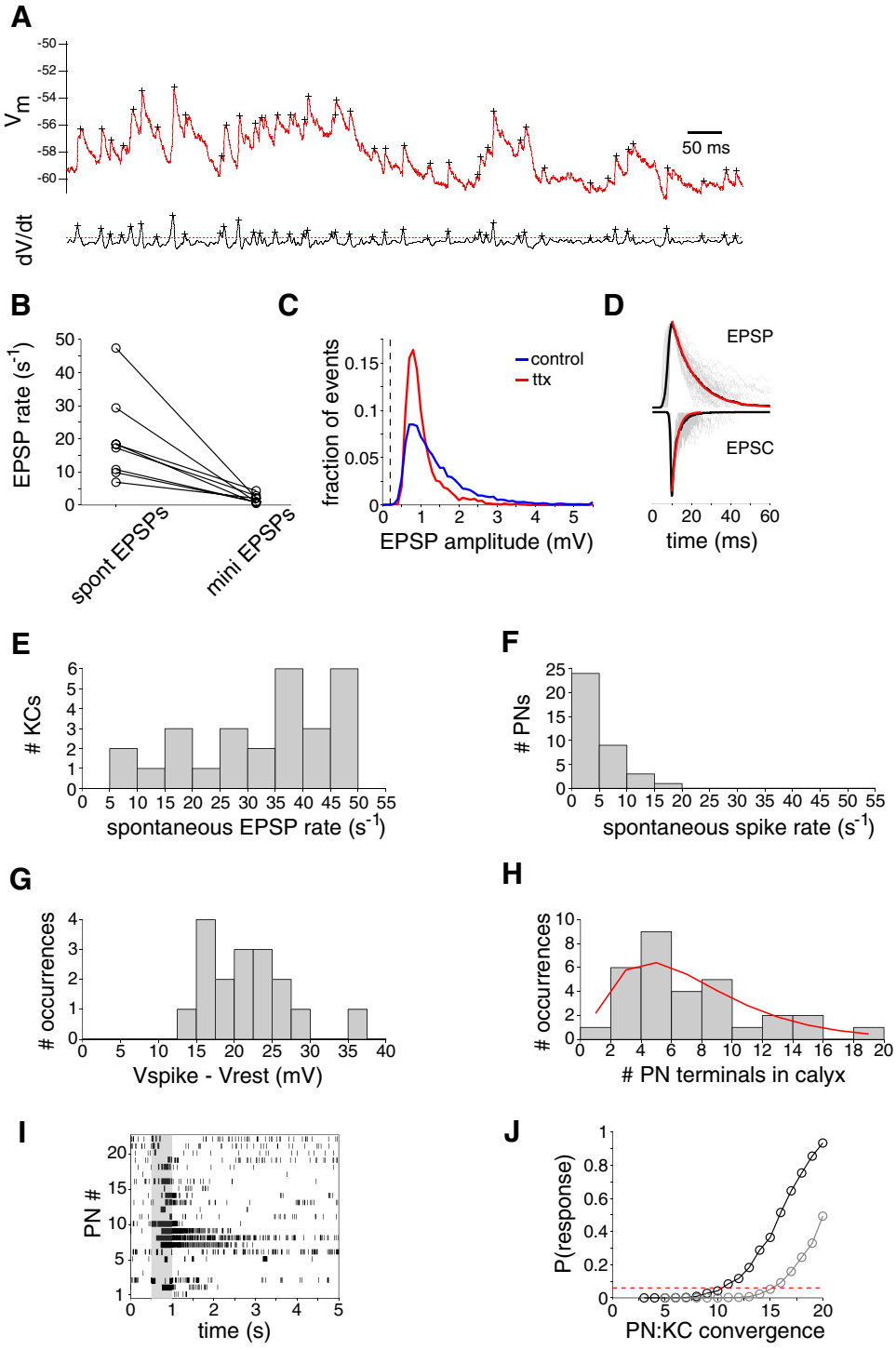

FIG. 3. Synaptic input to *Drosophila* KCs. *A*: spontaneous excitatory postsynaptic potentials (EPSPs) are detected by finding peaks in the first time derivative of the membrane potential (red: V_m, black: dV_m/dt). *B*: rate of EPSPs before (spontaneous EPSPs) and after action-potential blockade with 1 μM TTX (miniature EPSPs). *C*: distribution of spontaneous and miniature EPSP amplitudes. The upper end of the distribution ranged to larger amplitudes for spontaneous EPSPs, consistent with the occurrence of multi-quantal events, but the smallest EPSP amplitudes are the same under the two conditions. *D*: average EPSP (*top*) and EPSC (*bottom*) waveforms (thick black line). Individual events are superimposed in gray, and the exponential fit to the falling phase shown in red. Synaptic kinetics are relatively rapid [mean EPSP 10–90% rise time = 2.1 ms; decay time constant = 11.5 ms; mean EPSC 10–90% rise time = 0.9 ms; decay time constant = 2.8 ms]. *E*: distribution of rates of spontaneous EPSP rates in KCs (32.6 ± 12.7 s^{-1}, n = 27 KCs). *F*: distribution of spontaneous spike rates in PNs (4.6 ± 4.2 s^{-1}, n = 37 PNs). *G*: distribution of difference between resting potential and threshold for odor-evoked spikes (21.5 ± 5.6 mV, n = 17 KCs). *H*: number of synaptic output terminals per PN in the mushroom body (7.2 ± 4.2 terminals, for 216 PNs representing 31 different glomeruli). Red line indicates fitted Γ probability density function. *I*: spiking responses of 23 different PNs to benzaldehyde presentation, indicated by gray bar. Responses are recorded in different flies and aggregated. *J*: relationship between response probability of conductance-based model KCs and PN:KC connectivity. The experimentally observed 6% response probability is indicated by the dashed red line. Black symbols indicate response probability obtained with mean EPSP amplitude (1.4 mV), gray with median EPSP amplitude (1.2 mV).

evoked EPSPs must result from the release of single quanta; the tail of the control distribution indicates that some spontaneous events contain multiple quanta, although they could also result from coincident inputs from more than one PN.

EPSP/EPSC KINETICS. EPSP kinetics were surprisingly fast for neurons with input resistance >10 GΩ (Fig. 3*D*). We examined the time course of 50 well-isolated EPSPs from seven independent recordings. EPSP 10–90% rise times were 2.1 ± 0.5 ms, and decays were well fit with a single exponential (11.5 ± 5.3 ms). We measured the kinetics of 50 EPSCs from voltage-clamp recordings (V_{hold} = −60 mV) in five different flies. EPSC rise time was 0.9 ± 0.4 ms, and decay time constant was 2.8 ± 1.2 ms (Fig. 3*D*). Although EPSP kinetics were fast, the membrane time constant, measured at the soma by hyperpolarizing current injection, was very long (>200 ms). These observations suggest that EPSP kinetics are determined mostly by synaptic (and possibly, voltage-gated) conductances in the dendrites.

ESTIMATING PN-KC CONVERGENCE. Focusing on stretches of baseline voltage, we measured the frequency *e* of spontaneous EPSPs in KCs (Fig. 3*E*: 32.6 ± 12.7 s^{-1}, n = 27 KCs; detected as in Fig. 3*A*) and compared it to the spontaneous PN firing rate *f*, measured in the same conditions (Fig. 3*F*: 4.6 ± 4.2 s^{-1}, n = 37 PNs). Because PNs are likely to be the sole source of excitatory inputs to KCs, and assuming that each spontaneous PN action potential causes an EPSP in its postsynaptic KCs, we can estimate average connectivity between PNs and KCs as the ratio *e*/*f*. This ratio is about seven PNs to one KC. This estimate is a lower bound, however: *e* is almost certainly underestimated in our measurements, and PN release probability is probably <1. In addition, the distribution of spontaneous events detected in KCs is wide and asymmetric, indicating that convergence ratios are probably also variable across PNs and KCs.

We made an independent estimate of PN-KC connectivity based on anatomical data. We estimated the total number of synapses made by PNs within the mushroom body and assumed that those outputs are divided among the population of ~2,500 KCs. The total number of PN outputs in the mushroom body is the product of three quantities: the number of PNs projecting to the mushroom body; the number of synaptic boutons per PN; and the number release sites per terminal. Approximately 150 PNs project to the mushroom body (Jefferis et al. 2007). Each PN extends several axon collaterals into the mushroom body that each terminate in large synaptic boutons. The distribution of numbers of boutons made, in the calyx, by PNs with dendrites in 31 of the 50 glomeruli (216 PNs in toto) is shown in Fig. 3*H* (Jefferis et al. 2007). We fit this distribution with a Γ probability density function, and from it estimate that there are about 1,115 boutons for a population of 150 PNs. PN boutons are relatively large (2–7 μm in diameter), and each makes synapses onto several dendritic profiles (Yasuyama et al. 2002). Here we assume that each profile corresponds to a different KC, which may lead to an overestimate of PN:KC convergence. To estimate the number of synapses per bouton, we refer to electron microscopic observations of PN active zones (Yasuyama et al. 2002). In one section of one PN bouton, Yasuyama et al. found seven active zones. Assuming an average bouton diameter of 4 μm, those seven active zones would be distributed along a perimeter of 12.6 μm with 1.8 μm average spacing between active zones. Tiling the surface of a spherical 4-μm-diam bouton with this density yields ~30 active zones per bouton. These figures predict that there are 33,450 PN synapses in the MB, for an average of 13 PNs per KC. Thus our two independent measures of connectivity give a PN:KC convergence ratio of around 10:1 or 5% on average, with a likely range of 5:1 to 15:1.

TESTING OUR ESTIMATES OF CONVERGENCE. Could we, using such PN:KC convergence ratios, reproduce the observed 6% response probability in a model KC population, driven by odor-evoked PN spiking patterns? We simulated a population of 1,000 conductance-based model KCs with only passive membrane properties, randomly connected to an input layer of 23 PNs, with a fixed PN:KC convergence ratio. Activity profiles for these 23 PNs were taken directly from the recorded responses of 23 PNs to the odor benzaldehyde (Fig. 3*I*). These 23 PNs are an extensive sample of the ~50 different PN types found in the *Drosophila* antennal lobe. We next examined the relationship between KC response probability and convergence ratio.

Model EPSP kinetics were tuned to match experimental data, and model unitary EPSP amplitude was chosen to be either the mean (1.4 mV) or the median (1.2 mV) of the experimental distribution (Fig. 3*C*). KC spiking thresholds were measured from experiments by analyzing odor responses that contained four or fewer action potentials. Threshold was defined as the peak of the second time derivative of the membrane potential trace. The difference between resting potential and spike threshold is shown for 17 KCs in Fig. 3*G* (21.5 ± 5.6 mV). The average holding potential for the KCs was −57.8 mV; thus we set the voltage threshold for our model KCs at −36.3 mV. We found that, with connectivity ratios around 10:1, and an EPSP amplitude of 1.4 mV, our model matched closely the experimental KC response probability of 6% (Fig. 3*J*). When EPSP size was decreased to match the median value of 1.2 mV, a higher connectivity ratio of 15:1 was required to achieve the same response probability (gray curve in Fig. 3*J*). Thus a simple KC model based entirely on experimental data for EPSP amplitude, EPSP kinetics, KC firing threshold and PN response profiles, produces the observed KC response probabilities within the appropriate range of PN:KC convergence ratios.

PERIODICITY OF INPUTS. In locust, odor-evoked PN population output is oscillatory (Laurent and Davidowitz 1994) (Fig. 4*A*, *top*), due to fast inhibitory feedback in the antennal lobe (MacLeod and Laurent 1996). Consequently, periodicity (20–30 Hz) can be seen in intracellular KC membrane voltage recordings and in power spectra or autocorrelation functions calculated from these traces (Fig. 4*A*) (see also Jortner et al. 2007; Laurent and Naraghi 1994; Perez-Orive et al. 2002). In locust, each period of synaptic drive to a KC is composed of alternating volleys of direct excitation from PNs and delayed feedforward inhibition via a small group of GABAergic neurons in the lateral horn (Perez-Orive et al. 2002). These oscillation cycles define short and periodic synaptic integration windows for KCs, contributing to their high odor specificity (Perez-Orive et al. 2002). We analyzed *Drosophila* KC membrane potential fluctuations during odor stimulation. We could find no significant evidence for consistent periodicity in these traces (Fig. 4, *B–D*). These results alone do not rule out the possible

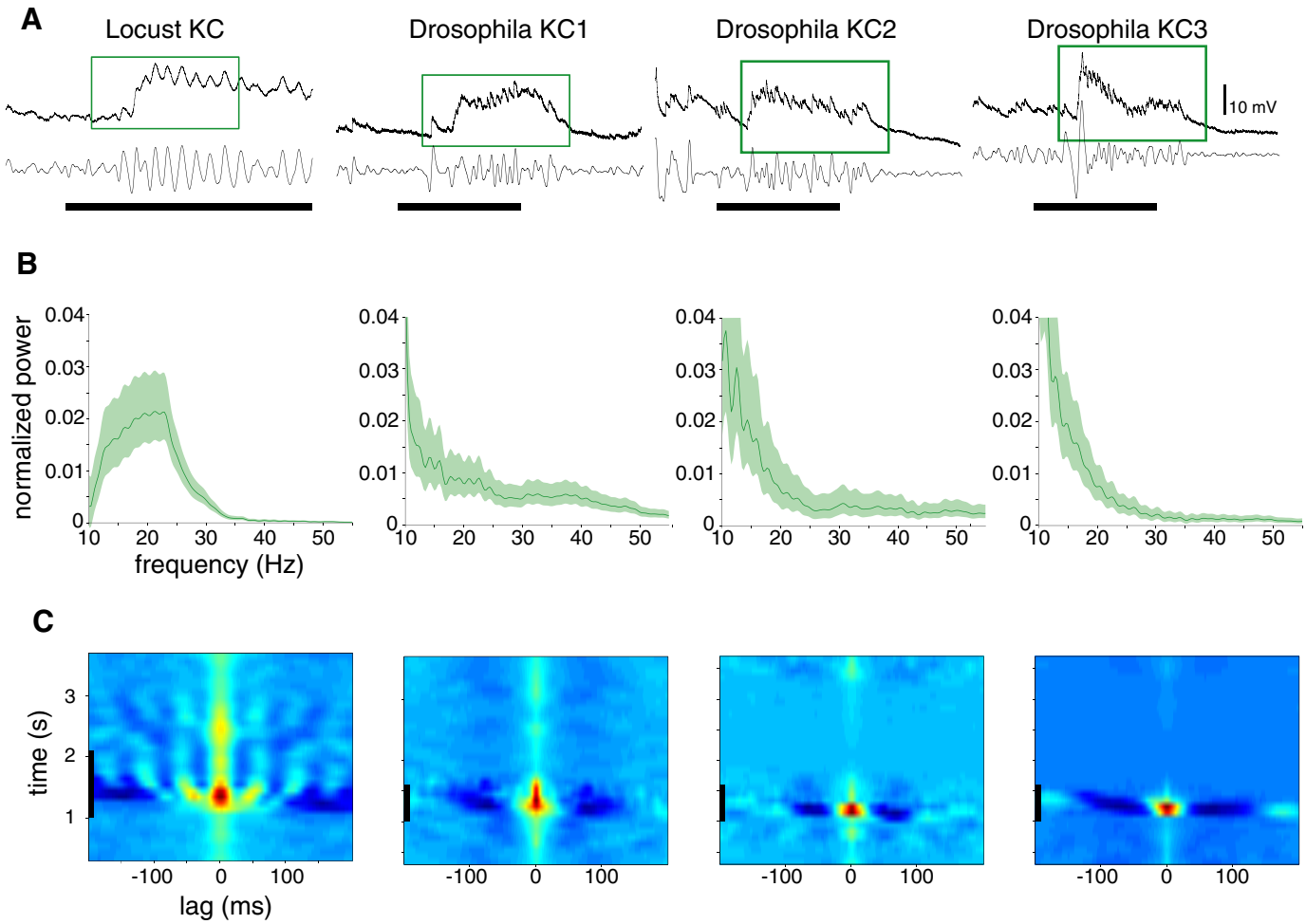

FIG. 4. Periodicity of synaptic inputs to KCs in locust and *Drosophila*. *A*: odor response of a locust KC and three different *Drosophila* KCs. *Top trace*: raw V_m; *bottom trace*: filtered from 10 to 55 Hz. Black bar indicates timing of odor delivery, green boxes indicate time window for power spectral density analysis. *B*: power spectral density (PSD) of odor-evoked power in KC membrane potential. Odor-evoked PSD is the difference in power during the excitatory response (green box in *A*) relative to power 10 s after odor presentation. PSD values are averaged over multiple odor trials, shading represents 1% confidence intervals. *C*: autocorrelation over time of 2–55 Hz filtered KC membrane potential, odor delivery indicated by black bar. In locust, odor-evoked oscillations with a 50-ms period produce periodic structure in the autocorrelogram. In *Drosophila,* autocorrelation values are high at odor onset because of the strong DC response to odor, but there is no evidence of periodic activity.

existence of synchronized (periodic or not) PN output. Because PN convergence to each KC is low, periodicity might also be difficult to detect from such recordings. Definitive evidence will require simultaneous recordings from multiple PNs during odor responses.

Does sparsening decrease overlap between representations?

Sparse representations are useful in memory networks for at least two related reasons (Kanerva 1988; Marr 1969; Olshausen and Field 2004; Tsodyks 1988): if an item is represented by relatively few neurons, memorization of this item requires the modification of only a few synaptic nodes; if representations are sparse, overlap and thus the probability of synaptic interference is reduced. As a corollary, sparse representations can be more easily separated because their overlap is reduced: sparsening, if done well, decorrelates representations (Laurent 2002; Perez-Orive et al. 2002). The *Drosophila* olfactory system affords a chance to test this directly: we predicted that the representations of different odors by the KC population should be more separable than they are in upstream layers where representations are denser. We thus compared the discriminability of population responses to a panel of eight different odors in KCs and in OSNs.

For this comparison, we obtained a new KC dataset (Fig. 5), where odors were delivered at a slightly higher concentration, to match the stimulus conditions where OSNs have been recently characterized (Hallem and Carlson 2006). We recorded the responses of 40 KCs to a panel of eight odors (6 trials each) under these conditions. KC population activity evoked by each odor was characterized as a 40-dimensional vector, where each dimension represents the mean firing rate of one KC during odor presentation. We used published data (Hallem and Carlson 2006) to construct corresponding population vectors with 24 OSN types (4–6 trials). For each odor pair, we compared the angle separating the two KC vectors (one for each odor) to that between the two corresponding OSN vectors.

Angular separation is a measure of correlation, however, in this context it has a biological interpretation: it reflects the ability of a network to learn to discriminate different inputs by

adjusting synaptic weights appropriately. In formal two-layered neural network models, activity at the output layer is usually calculated as the dot product between an input activity vector and a matrix of synaptic weights. Discrimination between input vectors is optimized by gradual modification of synaptic weights. It follows that the angle between different input vectors is important for stimulus discrimination: if two input vectors are separated by a small angle, only few synaptic weight matrices will improve separation. If input vectors are widely separated, however, finding appropriate sets of synaptic weights is relatively easy. Hence angular separation between input vectors directly relates to how effectively plasticity in the network can optimize discrimination.

All pair-wise separation values [1-cos(α), where α is the angle defined by the two vectors] between odor vectors are shown in Fig. 5*A* in OSN and KC spaces. Overall, distances were significantly greater between KC vectors than between OSN vectors (Fig. 5*B;* *t*-test : $P < 10^{-7}$). Separation was greater in KC space for 24 of the 28 possible odor pairs (Fig. 5*C;* Wilcoxon signed-rank test: $P = 10^{-4}$). Vector separation decreased for only four odor pairs; all such pairs included the odor methyl salicylate. OSN tuning to methyl salicylate happens to be unusually narrow: only 1 of the 24 OSNs (expressing Or10a) responds to this odor with a firing rate >50 Hz (Hallem and Carlson 2006). Consequently, the representation of methyl salicylate is far less distributed among OSNs than it is for all other odors tested. The decrease in separation of this odor's representation from the others may reflect the ultimate convergence of multiple OSN channels onto individual KCs. Altogether, these results indicate that odor separability is, as hypothesized, greater overall in the sparsely activated KC population than it is in the OSN array.

To further examine the transformations of representations from OSNs to KCs, we tested whether KC response profiles might be derived simply by thresholding the tuning curve of any of the 24 well-characterized OSNs (Hallem and Carlson 2006). Of the 22 KCs (among 111 KCs in our entire data set) that responded to two or more odors, this was possible with only 4 KC response profiles (Fig. 5*D*). This analysis included only 24 of the ~60 total OSN tuning curves, raising the possibility that the 18 unmatched KC tuning profiles correspond to the 37 uncharacterized OSN profiles. However, the probability that, in a sample of 22 KCs, 18 are from this set of uncharacterized OSNs can be calculated from the cumulative binomial probability distribution; this probability is 0.008. This mismatch between KC and OSN tuning profiles indicates that KC responses cannot be explained by simple thresholding of labeled-line channels from OSNs; rather, KC response profiles probably result from the previously documented broadening of PN tuning profiles (Wilson et al. 2004) together with convergence of multiple PN inputs.

DISCUSSION

Olfactory networks—like all sensory systems—face the complex problem of generating representations in a format appropriate for detection, discrimination, storage, and recall. Optimizing odor representations for memorization should satisfy at least three requirements: appropriate capacity, ease of storage and recall accuracy. Insect olfactory systems are ideal to study these forms of computational optimization. In fruit flies, odor representations by OSNs are distributed and combinatorial (Hallem and Carlson 2006; Hallem et al. 2006). In the antennal lobe, PNs that respond to nonpheromonal odors are more broadly tuned than their cognate OSNs (Schlief and Wilson 2007; Wilson et al. 2004). Such distributed codes endow this network with a high representational capacity. At the same time, because combinatorial codes use each individual neuron in the representation of many inputs, they impose distributed formats for memorization also and thus increase the chance of interference between memories. The transformation to sparse representations in the mushroom body may represent one solution to this problem.

We presented evidence that the representations of odors by *Drosophila* mushroom body neurons are sparse and that overlap between different representations is significantly less in the mushroom body than it is in the receptor layer. Although sparseness has long been proposed to be useful for learning and memory, this is the first direct experimental evidence indicating that the olfactory network could learn to discriminate odors more readily by adjusting synaptic weights at the KC layer than at the OSNs. Simple thresholding of individual OSN channels can probably not explain KC response profiles ($P < 0.01$). Individual KCs receive inputs from ~10 PNs on average. Because there are only two to five PNs per antennal lobe glomerulus, each KC must receive convergent inputs from multiple glomeruli. This convergence, combined with reshaping of tuning profiles in the antennal lobe (Wilson et al. 2004), could enable KCs to represent a wide variety of odors however complex their composition, even though responses are sparse. Such a design requires that KCs vastly outnumber their input channels, consistent with observations with all studied insect species (Strausfeld et al. 1998).

We described the synaptic mechanisms that shape KC odor response profiles and found them to differ from those used in a distantly related species, the locust (Perez-Orive et al. 2002). This indicates that different integration schemes may be used to achieve a similar transformation to sparse encoding. It also suggests that this transformation, because it is common to these two species, may be a fundamental requirement of these types of circuit. The mechanistic differences between species may, however, also have interesting implications for each system's capacity. We now discuss these results.

Transformation of olfactory representations in the Drosophila mushroom body

The tuning profiles of a large fraction (24 of 60) of all the OSNs have been well characterized in *Drosophila* by John Carlson and colleagues (Hallem and Carlson 2006). By comparing these with our characterizations of KCs, we could test whether the overlap between odor representations diminishes as signals flow through olfactory circuits. To measure the degree of overlap, we constructed population activity vectors for eight odors, with sets of 24 OSNs and 40 KCs; we then compared the distribution of correlations between those vectors calculated with OSNs to those in the KC population. Overall, representations were significantly better separated in the mushroom body than in the receptor layer. A combination of sparseness and good representation separability is highly desirable for memory systems (Garcia-Sanchez and Huerta 2003; Huerta et al. 2004; Kanerva 1988; Olshausen and Field 2004;

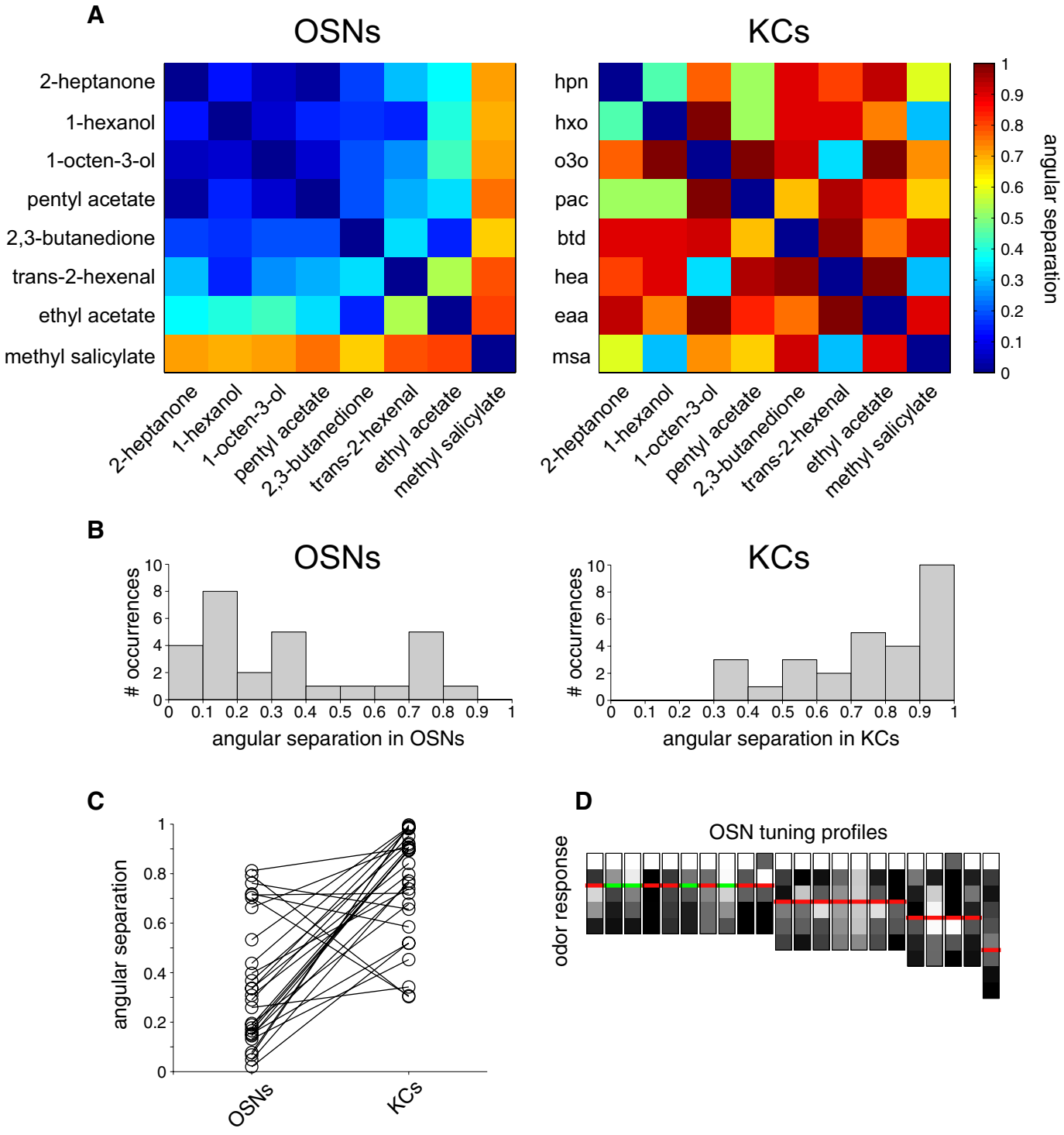

FIG. 5. Separation of odors in olfactory sensory neuron and KC populations. *A*: angular separation between population vectors representing different pairs of odors in sensory neurons (OSNs, *left*) and KCs (right). Vectors comprised the mean responses of 24 OSNs or 40 KCs, and angular separation was calculated as 1-cos(α) where α is the angle between a pair of vectors. Odors ordered by rank in OSN space. *B*: angular separation values for all pairs of the 8 odors in *A*. Separation values for OSNs are shown on the *left,* for KCs on the *right. C*: change in angular separation values between OSNs and KCs. Separation values for each pair of odors in OSNs are plotted on the *left,* and the corresponding values in the KCs are on the *right.* Twenty-four of 28 pairs of odors have greater angular separation in KC space ($P = 10^{-4}$, Wilcoxon signed-rank test). *D*: OSN tuning profiles that best match KC profiles. For 22 KCs that responded to ≥2 odors, a closely matching OSN tuning profile was identified. Each column represents an OSN tuning profile, where each square displays the normalized response intensity to a particular odor (response intensity decreasing from white to black). OSN tuning profiles are arranged so odors that evoke a response in the KC are above the green or red line, and 3 odors that fail to evoke a response are below the line. These 3 odors are arranged in order of descending response intensity in the OSN. Thus an OSN tuning profile that monotonically decreases down the column can be thresholded to generate a KC tuning profile; these thresholds are shown in green. OSN tuning profiles that are not monotonic cannot be simply thresholded to generate a KC profile, as indicated by the red lines.

Tsodyks and Feigel′man 1988; Willshaw and Lonquet-Higging 1969) and consistent with the role assigned to mushroom bodies (de Belle and Heisenberg 1994; Hammer and Menzel 1998).

Drosophila KCs can be classified into three types, based on axonal projections and birth order (Crittenden et al. 1998; Lee et al. 1999; Strausfeld et al. 2003): γ KCs are born first and have a single medially projecting axon; α'/β' KCs are born second and α/β KCs last; both types have bifurcating axons with both medial and dorsal projections. Genetic and behavioral studies, exploiting selective blockade of synaptic release from individual KC classes suggest that these KC types are differentially involved in olfactory learning and memory (Akalal et al. 2006; Pascual and Preat 2001; Zars et al. 2000). Recent work, for example, indicates that α'/β' KCs are involved in memory acquisition (Krashes et al. 2007). Our results indicate that there are small but notable physiological differences between KC subtypes: in a sample of 71 KCs, we found there was a trend for tuning widths to decrease from α'/β' to α/β to γ KCs, although the only statistically significant difference was between α'/β' and γ KCs. α'/β' KCs also had the largest baseline- and response-firing rates. As the most responsive KC types, α'/β' neurons might be the ones most likely to experience spike-timing dependent plasticity (Cassenaer and Laurent 2007), which could account for their involvement in memory acquisition.

Mechanisms for sparsening in Drosophila mushroom bodies

To investigate synaptic integration by *Drosophila* KCs, we characterized EPSP amplitudes, EPSP/C kinetics and PN:KC connectivity. EPSPs recorded from somata were quite large: 1.4 ± 0.8 mV. EPSPs rose and decayed rapidly, a corollary of fast EPSC kinetics, consistent with in vitro recordings (Gu and O'Dowd 2006). We estimated PN:KC convergence using two independent methods. The first, based on electrophysiological measurements, suggested an average of 7:1. The second, based on available anatomical data (Jefferis et al. 2007; Yasuyama et al. 2002), suggested an average of 13:1. Based on these estimates, we propose that PN:KC convergence in *Drosophila* is distributed about a mean of 10:1 with a likely range between 5:1 and 15:1. Using these parameters, we could simulate a layer of conductance-based model KCs and reproduce responses to PN input with sparseness consistent with experiments. This input was taken from the odor responses of 23 PNs, a significant sample of the ~50 different PN types in the *Drosophila* antennal lobe. Hence in *Drosophila*, low PN convergence combined with rapid EPSP kinetics and appropriately high KC firing thresholds appear sufficient to generate sparse KC responses.

Comparative aspects

We can now compare circuits, formats and mechanisms of olfactory computation between two insect species— the locust, a hemimetabolous orthopteran and the fruit fly, a holometabolous dipteran—separated by >300 million years of evolution. The most striking common features are the dense, distributed odor representations in the antennal lobes and the sparse, distributed representations of those same odors in the mushroom bodies: mean response probability drops from 64% in PNs to 11% in KCs in locust (Perez-Orive et al. 2002), and from 59 to 6% in *Drosophila* (this paper). This consistency suggests that there is a strong selective pressure to generate sparse representations in the mushroom bodies. We propose that sparsening is an intrinsic requirement of such memory systems (Broome et al. 2006; Laurent 2002; Perez-Orive et al. 2002).

Although sparsening is common to both species, the mechanisms to achieve it appear to be quite distinct. In locust, sparseness is achieved in part because temporal integration by KCs is curtailed: PN input to KCs is composed of periodic excitation and phase-lagged inhibition, defining repeated short (25 ms) integration windows separated by voltage-resetting inhibitory postsynaptic potentials (IPSPs) (Perez-Orive et al. 2002). These volleys occur periodically at a frequency of ~20 Hz, generating synchronized oscillations in the KC membrane potential (Laurent and Naraghi 1994; Perez-Orive et al. 2002). This periodic integration scheme is essential because PN-to-KC convergence is extremely high [~50% or ~400 PNs per KC (Jortner et al. 2007)] relative to the number of simultaneous PN inputs required to bring a KC to threshold (<70) (Jortner et al. 2007). Without periodic voltage-resetting IPSPs, KCs lose their odor selectivity because temporal integration becomes possible (Perez-Orive et al. 2002).

In *Drosophila*, by contrast, PN:KC convergence is low (~5% or ~10 PNs per KC) relative to the minimum number of EPSPs needed to get a KC to spike (15 inputs minimum: 21.5 mV from V_{rest} to V_{spike}, 1.4 mV EPSP amplitude). This implies a need for input amplification and/or temporal summation. Indeed we find no evidence for a periodic voltage reset by IPSPs, as seen in locust, allowing considerable temporal integration by KCs.

Note that the lack of evidence for periodic synaptic input to KCs in *Drosophila* does not rule out the possibility that PN output is, as in locust (Laurent and Naraghi 1994; Wehr and Laurent 1996), periodic and/or synchronized: given the low PN:KC convergence in *Drosophila*, the membrane potential of individual KCs may not reflect well the average discharge statistics of the PN population. Neither PN nor LN recordings in the *Drosophila* antennal lobe indicate prominent periodicity in their odor responses (Olsen et al. 2007; Schlief and Wilson 2007; Wilson and Laurent 2005; Wilson et al. 2004); still, a definite answer will require simultaneous recordings from multiple PNs.

Do these mechanistic differences have any functional significance? Both mechanisms achieve similar goals: they sparsen odor representations in the mushroom body. Yet the differences could have important consequences for the representational capacity of each species. A key difference lies with PN:KC convergence ratios and neuron population sizes: with ~50,000 KCs and 50% convergence, locust mushroom bodies could, in principle, generate and store vastly more input combinations than *Drosophila*. If true, we would predict that olfactory circuit design is correlated with these global attributes. One interesting possibility is that oscillatory synchronization is correlated with high convergence ratios: with large fan-in, constraining temporal integration is essential for generating sparseness, as in the locust, whereas in systems with low convergence, such as *Drosophila,* sparseness can be achieved without oscillations.

Even with low fan-in, *Drosophila* KCs likely integrate information from multiple antennal lobe glomeruli. With 10 to 1 convergence, and between two and five PNs per glomerulus, a KC would receive input from at least two glomeruli if all the PNs from the same glomerulus connect to the same target KC and most likely more, especially if pairwise connections are not precisely specified. This convergence of glomerular channels, combined with processing in the antennal lobe (Olsen et al. 2007; Wilson et al. 2004), could increase the diversity of tuning profiles in the KC population relative to the earlier stages of the pathway. This is consistent with the diversity of tuning profiles we observe here and with our demonstration that KC tuning profiles cannot be generated simply by thresholding tuning profiles of individual OSNs. Although diverse, these tuning profiles are also odor specific. This combination of operations diminishes overlap between representations of different stimuli while maintaining high capacity, useful features for a network involved in learning and memory.

ACKNOWLEDGMENTS

We gratefully acknowledge and thank R. Wilson for providing PN data, E. Hallem and J. Carlson for OSN data, and G. Jefferis for anatomical data on PN bouton numbers. We thank the Caltech Biological Imaging Center for the use of their confocal microscopy facilities. We thank members of the Laurent lab, including V. Jayaraman, M. Murthy, A. Narayan, and R. Wilson, for valuable discussions.

Present address of G. C. Turner: Cold Spring Harbor Laboratory, 1 Bungtown Rd., Cold Spring Harbor NY 11724.

GRANTS

This work was supported by grants from the National Institute of Deafness and Other Communications Disorders to M. Bazhenov and G. Laurent, the National Science Foundation-Biological Information Technology and Systems Program, and the Lawrence Hanson Fund to G. Laurent. G. Turner was funded by the Jane Coffin Childs foundation and a Swartz foundation grant.

REFERENCES

Akalal DB, Wilson CF, Zong L, Tanaka NK, Ito K, Davis RL. Roles for *Drosophila* mushroom body neurons in olfactory learning and memory. *Learn Mem* 13: 659–668, 2006.

Bazhenov M, Stopfer M, Rabinovich M, Huerta R, Abarbanel HD, Sejnowski TJ, Laurent G. Model of transient oscillatory synchronization in the locust antennal lobe. *Neuron* 30: 553–567, 2001.

Broome BM, Jayaraman V, Laurent G. Encoding and decoding of overlapping odor sequences. *Neuron* 51: 467–482, 2006.

Cassenaer S, Laurent G. Hebbian STDP in mushroom bodies facilitates the synchronous flow of olfactory information in locusts. *Nature* 448: 709–713, 2007.

Clyne P, Grant A, O'Connell R, Carlson JR. Odorant response of individual sensilla on the *Drosophila* antenna. *Invert Neurosci* 3: 127–135, 1997.

Clyne PJ, Warr CG, Freeman MR, Lessing D, Kim J, Carlson JR. A novel family of divergent seven-transmembrance proteins: candidate odorant receptors in *Drosophila. Neuron* 22: 327–338, 1999.

Crittenden JR, Skoulakis EM, Han KA, Kalderon D, Davis RL. Tripartite mushroom body architecture revealed by antigenic markers. *Learn Mem* 5: 38–51, 1998.

de Belle JS, Heisenberg M. Associative odor learning in *Drosophila* abolished by chemical ablation of mushroom bodies. *Science* 263: 692–695, 1994.

de Bruyne M, Clyne PJ, Carlson JR. Odor coding in a model olfactory organ: the *Drosophila* maxillary palp. *J Neurosci* 19: 4520–4532, 1999.

de Bruyne M, Foster K, Carlson JR. Odor coding in the *Drosophila* antenna. *Neuron* 30: 537–552, 2001.

Destexhe A, Mainen ZF, Sejnowski TJ. Synthesis of models for excitable membranes, synaptic transmission and neuromodulation using a common kinetic formalism. *J Comput Neurosci* 1: 195–230, 1994.

Dobritsa AA, van der Goes van Naters W, Warr CG, Steinbrecht RA, Carlson JR. Integrating the molecular and cellular basis of odor coding in the *Drosophila* antenna. *Neuron* 37: 827–841, 2003.

Dubnau J, Grady L, Kitamoto T, Tully T. Disruption of neurotransmission in *Drosophila* mushroom body blocks retrieval but not acquisition of memory. *Nature* 411: 476–480, 2001.

Erber J, Masuhr T, Menzel R. Localization of short-term memory in the brain of the bee, *Apis mellifera. Physiol Entomol* 5: 343–358, 1980.

Gao Q, Chess A. Identification of candidate *Drosophila* olfactory receptors from genomic DNA sequence. *Genomics* 60: 31–39, 1999.

Garcia-Sanchez M, Huerta R. Design parameters of the fan-out phase of sensory systems. *J Comput Neurosci* 15: 5–17, 2003.

Goodman MB, Lockery SR. Pressure polishing: a method for re-shaping patch pipettes during fire polishing. *J Neurosci Methods* 100: 13–15, 2000.

Gu H, O'Dowd DK. Cholinergic synaptic transmission in adult *Drosophila* Kenyon cells in situ. *J Neurosci* 26: 265–272, 2006.

Ha TS, Smith DP. A pheromone receptor mediates 11-cis-vaccenyl acetate-induced responses in *Drosophila. J Neurosci* 26: 8727–8733, 2006.

Hallem EA, Carlson JR. Coding of odors by a receptor repertoire. *Cell* 125: 143–160, 2006.

Hallem EA, Dahanukar A, Carlson JR. Insect odor and taste receptors. *Annu Rev Entomol* 51: 113–135, 2006.

Hammer M, Menzel R. Multiple sites of associative odor learning as revealed by local brain microinjections of octopamine in honeybees. *Learn Mem* 5: 146–156, 1998.

Han KA, Millar NS, Davis RL. A novel octopamine receptor with preferential expression in *Drosophila* mushroom bodies. *J Neurosci* 18: 3650–3658, 1998.

Han KA, Millar NS, Grotewiel MS, Davis RL. DAMB, a novel dopamine receptor expressed specifically in *Drosophila* mushroom bodies. *Neuron* 16: 1127–1135, 1996.

Han PL, Levin LR, Reed RR, Davis RL. Preferential expression of the *Drosophila rutabaga* gene in mushroom bodies, neural centers for learning in insects. *Neuron* 9: 619–627, 1992.

Heisenberg M, Borst A, Wagner S, Byers D. Drosophila mushroom body mutants are deficient in olfactory learning. *J Neurogenet* 2: 1–30, 1985.

Huerta R, Nowotny T, Garcia-Sanchez M, Abarbanel HD, Rabinovich MI. Learning classification in the olfactory system of insects. *Neural Comput* 16: 1601–1640, 2004.

Jayaraman V, Laurent G. Evaluating a genetically encoded optical sensor of neural activity using electrophysiology in intact adult fruit flies. *Front Neural Circuits* In press.

Jefferis GS, Potter CJ, Chan AM, Marin EC, Rohlfing T, Maurer CR II, Luo L. Comprehensive maps of *Drosophila* higher olfactory centers: spatially segregated fruit and pheromone representation. *Cell* 128: 1187–1203, 2007.

Jortner RA, Farivar SS, Laurent G. A simple connectivity scheme for sparse coding in an olfactory system. *J Neurosci* 27: 1659–1669, 2007.

Kanerva P. *Sparse Distributed Memory.* Cambridge, MA: MIT Press, 1988.

Krashes MJ, Keene AC, Leung B, Armstrong JD, Waddell S. Sequential use of mushroom body neuron subsets during *Drosophila* odor memory processing. *Neuron* 53: 103–115, 2007.

Laurent G. A systems perspective on early olfactory coding. *Science* 286: 723–728, 1999.

Laurent G. Olfactory network dynamics and the coding of multidimensional signals. *Nat Rev Neurosci* 3: 884–895, 2002.

Laurent G, Davidowitz H. Encoding of olfactory information with oscillating neural assemblies. *Science* 265: 1872–1875, 1994.

Laurent G, Naraghi M. Odorant-induced oscillations in the mushroom bodies of the locust. *J Neurosci* 14: 2993–3004, 1994.

Lee T, Lee A, Luo L. Development of the *Drosophila* mushroom bodies: sequential generation of three distinct types of neurons from a neuroblast. *Development* 126: 4065–4076, 1999.

Lewis EB. A new standard food medium. *Drosophila Information Service* 34: 117–118, 1960.

Lockery SR, Goodman MB. Tight-seal whole-cell patch clamping of *Caenorhabditis elegans* neurons. *Methods Enzymol* 293: 201–217, 1998.

Logothetis NK, Sheinberg DL. Visual object recognition. *Annu Rev Neurosci* 19: 577–621, 1996.

MacLeod K, Laurent G. Distinct mechanisms for synchronization and temporal patterning of odor-encoding neural assemblies. *Science* 274: 976–979, 1996.

Marr D. A theory of cerebellar cortex. *J Physiol* 202: 437–470, 1969.

McGuire SE, Le PT, Davis RL. The role of *Drosophila* mushroom body signaling in olfactory memory. *Science* 293: 1330–1333, 2001.

Nighorn A, Healy MJ, Davis RL. The cyclic AMP phosphodiesterase encoded by the *Drosophila dunce* gene is concentrated in the mushroom body neuropil. *Neuron* 6: 455–467, 1991.

Olsen SR, Bhandawat V, Wilson RI. Excitatory interactions between olfactory processing channels in the *Drosophila* antennal lobe. *Neuron* 54: 89–103, 2007.

Olshausen BA, Field DJ. Sparse coding of sensory inputs. *Curr Opin Neurobiol* 14: 481–487, 2004.

Pascual A, Preat T. Localization of long-term memory within the *Drosophila* mushroom body. *Science* 294: 1115–1117, 2001.

Perez-Orive J, Mazor O, Turner GC, Cassenaer S, Wilson RI, Laurent G. Oscillations and sparsening of odor representations in the mushroom body. *Science* 297: 359–365, 2002.

Pologruto TA, Yasuda R, Svoboda K. Monitoring neural activity and [Ca^{2+}] with genetically encoded Ca^{2+} indicators. *J Neurosci* 24: 9572–9579, 2004.

Python F, Stocker RF. Immunoreactivity against choline acetyltransferase, gamma-aminobutyric acid, histamine, octopamine, and serotonin in the larval chemosensory system of *Dosophila melanogaster*. *J Comp Neurol* 453: 157–167, 2002.

Quiroga RQ, Reddy L, Kreiman G, Koch C, Fried I. Invariant visual representation by single neurons in the human brain. *Nature* 435: 1102–1107, 2005.

Robertson HM, Warr CG, Carlson JR. Molecular evolution of the insect chemoreceptor gene superfamily in *Drosophila melanogaster*. *Proc Natl Acad Sci USA* 100, *Suppl* 2: 14537–14542, 2003.

Schlief ML, Wilson RI. Olfactory processing and behavior downstream from highly selective receptor neurons. *Nat Neurosci* 10: 623–630, 2007.

Schwaerzel M, Heisenberg M, Zars T. Extinction antagonizes olfactory memory at the subcellular level. *Neuron* 35: 951–960, 2002.

Shang Y, Claridge-Chang A, Sjulson L, Pypaert M, Miesenbock G. Excitatory local circuits and their implications for olfactory processing in the fly antennal lobe. *Cell* 128: 601–612, 2007.

Stopfer M, Jayaraman V, Laurent G. Intensity versus identity coding in an olfactory system. *Neuron* 39: 991–1004, 2003.

Strausfeld NJ, Hansen L, Li Y, Gomez RS, Ito K. Evolution, discovery, and interpretations of arthropod mushroom bodies. *Learn Mem* 5: 11–37, 1998.

Strausfeld NJ, Sinakevitch I, Vilinsky I. The mushroom bodies of *Drosophila melanogaster*: an immunocytological and golgi study of Kenyon cell organization in the calyces and lobes. *Microsc Res Tech* 62: 151–169, 2003.

Suh GS, Wong AM, Hergarden AC, Wang JW, Simon AF, Benzer S, Axel R, Anderson DJ. A single population of olfactory sensory neurons mediates an innate avoidance behavior in *Drosophila*. *Nature* 431: 854–859, 2004.

Tanaka K. Inferotemporal cortex and object vision. *Annu Rev Neurosci* 19: 109–139, 1996.

Tsodyks MV, Feigel'man MV. The enhanced storage capacity in neural networks with low activity level. *Europhys Lett* 6: 101–105, 1988.

Tully T, Preat T, Boynton SC, Del Vecchio M. Genetic dissection of consolidated memory in *Drosophila*. *Cell* 79: 35–47, 1994.

van der Goes van Naters W, Carlson JR. Receptors and neurons for fly odors in *Drosophila*. *Curr Biol* 17: 606–612, 2007.

Vosshall LB, Amrein H, Morozov PS, Rzhetsky A, Axel R. A spatial map of olfactory receptor expression in the *Drosophila* antenna. *Cell* 96: 725–736, 1999.

Vosshall LB, Stocker RF. Molecular architecture of smell and taste in *Drosophila*. *Annu Rev Neurosci* 30: 505–533, 2007.

Wang JW, Wong AM, Flores J, Vosshall LB, Axel R. Two-photon calcium imaging reveals an odor-evoked map of activity in the fly brain. *Cell* 112: 271–282, 2003.

Wang Y, Guo HF, Pologruto TA, Hannan F, Hakker I, Svoboda K, Zhong Y. Stereotyped odor-evoked activity in the mushroom body of *Drosophila* revealed by green fluorescent protein-based Ca^{2+} imaging. *J Neurosci* 24: 6507–6514, 2004.

Wehr M, Laurent G. Odor encoding by temporal sequences of firing in oscillating neural assemblies. *Nature* 384: 162–166, 1996.

Willshaw D, Longuet-Higgins HC. Associative memory model. In: *Machine Intelligence*, edited by Meltzer B, Michie O. Edinburgh: University of Edinburgh Press, 1970.

Wilson RI, Laurent G. Role of GABAergic inhibition in shaping odor-evoked spatiotemporal patterns in the *Drosophila* antennal lobe. *J Neurosci* 25: 9069–9079, 2005.

Wilson RI, Turner GC, Laurent G. Transformation of olfactory representations in the *Drosophila* antennal lobe. *Science* 303: 366–370, 2004.

Xu P, Atkinson R, Jones DN, Smith DP. *Drosophila* OBP LUSH is required for activity of pheromone-sensitive neurons. *Neuron* 45: 193–200, 2005.

Yasuyama K, Meinertzhagen IA, Schurmann FW. Synaptic organization of the mushroom body calyx in *Drosophila melanogaster*. *J Comp Neurol* 445: 211–226, 2002.

Zars T, Fischer M, Schulz R, Heisenberg M. Localization of a short-term memory in *Drosophila*. *Science* 288: 672–675, 2000.